

# On the interpretation of echelle diagrams for solar-like oscillations Effect of centrifugal distortion

J.C. Suárez<sup>1,2</sup> and M.J. Goupil<sup>2</sup> and D.R. Reese<sup>2</sup> and R. Samadi<sup>2</sup> and F. Lignières<sup>3,4</sup> and  
M. Rieutord<sup>3,4</sup> and J. Lochard<sup>2</sup>

## ABSTRACT

This work aims at determining the impact of slow to moderate rotation on the regular patterns often present in solar-like oscillation spectra, i.e. the frequency spacings. We focus on the well-known asteroseismic diagnostic echelle diagrams, examining how rotation may modify the estimates of the large and small spacings, as well as the identification of modes. We illustrate the work with a real case: the solar-like star  $\eta$  Bootis.

We study a main sequence  $1.3M_{\odot}$  star as a typical case. The modeling takes into account rotation effects on the equilibrium models through an effective gravity and on the oscillation frequencies through both perturbative and non-perturbative calculations. We compare the results of both type of calculations in the context of the regular spacings (like the small spacings and the scaled small spacings) and echelle diagrams. We show that for echelle diagrams the perturbative approach remains valid for rotational velocities up to  $40 - 50 \text{ km s}^{-1}$ .

We show that for the rotational velocities measured in solar-like stars, i.e.  $v \sin i$  up to  $20 - 30 \text{ km s}^{-1}$ , rotation effects must be taken into account in the modeling for a correct interpretation of the observed oscillations. In particular, theoretical oscillation frequencies must be corrected up to the second-order in terms of rotation rate, including near degeneracy effects. For rotational velocities of about  $16 \text{ km s}^{-1}$  and higher, diagnostics on large spacings and on modal identification through echelle diagrams can be significantly altered by the presence of the  $m \neq 0$  components of the rotationally split modes. We found these effects to be detectable in the observed frequency range. Analysis of the effects of rotation on small spacings and scaled small spacings reveals that these can be of the order of, or even larger than surface effects, typically turbulence, microscopic diffusion, etc. Furthermore, we show that scaled spacings are significantly affected by stellar distortion even for small stellar rotational velocities (from  $10 - 15 \text{ km s}^{-1}$ ) and therefore some care must be taken when using them as indicators for probing deep stellar interiors.

*Subject headings:* stars: evolution –stars: individual( $\eta$  Bootis) — stars: interiors – stars: oscillations (including pulsations) stars: rotation –stars: solar-type

<sup>1</sup>Instituto de Astrofísica de Andalucía (CSIC), Granada, Spain.

<sup>2</sup>Observatoire de Paris, LESIA, CNRS UMR 8109, 92195 Meudon, France.

<sup>3</sup>Université de Toulouse, UPS, Laboratoire d'Astrophysique de Toulouse-Tarbes (LATT), 31400 Toulouse, France.

<sup>4</sup>CNRS, Laboratoire d'Astrophysique de Toulouse-Tarbes (LATT), 31400 Toulouse, France.

## 1. Introduction

Solar-like oscillations are detected in stars with outer convective zones, that is, in stars similar to the Sun (see Michel et al. 2008, and references therein) as well as in red giant stars (De Ridder et al. 2009) and even in massive B-type stars as recently shown by Belkacem et al. (2009). These oscillations are due to intrinsically stable pressure (p) modes which are excited by turbulent motions in the convective outer layers.

This stochastic process excites several modes in a star over a broad frequency range well above the fundamental radial mode frequency in a regime where frequencies show regular patterns in the power spectrum. This gives access to an information content based on different seismic signatures which may constrain fundamental stellar properties (namely mass, age, and radius) and probe the internal stellar structure to unprecedented accuracy (see, for instance, Gough 1987; Cunha & Metcalfe 2007; Teixeira et al. 2009).

On the other hand, the uninterrupted long observational runs required together with the expected small oscillation amplitudes has made the detection of solar-type stars technically challenging targets in particular, for asteroseismic space missions. A wealth of data is already available from *MOST* (Matthews 1998), *CoRoT* (Baglin 2003; Michel et al. 2008; Appourchaux et al. 2008; Belkacem et al. 2009) and *Kepler* (?).

Low mass stars are generally slow rotators (in most cases  $\langle v \sin i \rangle < 20 \text{ kms}^{-1}$ ) and the influence of rotation on the oscillation frequencies is globally small. For slow rotators, the geometrical structure is represented by a single spherical harmonics  $Y_\ell^m(\theta, \phi)$ , and the frequencies by  $\nu_{n,\ell,m}$  with  $n$  being the radial order of the mode. Rotation lifts the degeneracy causing the modes to split into  $m \neq 0$  multiplets. The  $m \neq 0$  are usually computed using a first-order perturbation formalism. Rotation also affects, indirectly, the  $m = 0$  mode frequencies as it modifies the internal structure through rotationally induced mixing (Goupil & Talon 2002; Mathis et al. 2007). In the same line, Carrier et al. (2005) studied the solar-like star  $\eta$  Bootis assuming a surface rotational velocity of about  $v_{\text{rot}} = 3 - 7 \text{ kms}^{-1}$ . The authors found that the effects of including rotationally-induced mixing was small and the rotation is not strong enough to impose a rigid rotation. In particular, they found that the core in this star rotates three times faster than the outer layers.

Distortion due to the centrifugal force can have a much larger impact on the oscillation frequencies even for slow rotators (see Goupil 2009, for a review on rotation effects on the oscillation frequencies). Such an effect is stronger for p modes with small inertia. These modes propagate mainly through the outer layers of the star. Therefore, their frequencies are more sensitive to changes in

the surface physical properties, where the centrifugal force becomes more efficient. The present work examines and evaluates the direct effects of rotation on the frequencies in this high-frequency domain, and its impact on the different seismic diagnostic techniques based on the asymptotic properties of the oscillations. More specifically, we analyze the case of different modes with close frequencies, such as  $\ell = 0$  and  $\ell = 2$ , which are systematically near degenerate. Since the small spacings are affected by near degeneracy, echelle diagrams, often used as a seismic diagnostic technique for solar-like stars, should also be affected.

We then first analyzed the effects of rotation on regular patterns observed in solar-like spectra, focusing on the small and large spacings, which are the most relevant quantities for echelle spectrograms. Even if solar-like stars are often slow rotators, their oscillation spectra show high-order frequencies, where the validity of perturbation theory for computing oscillation frequencies in absence of rotation might fail. This point was thus checked by comparing the perturbative calculations with recent non-perturbative calculations where the effect of rotation on the oscillations is fully taken into account (Reese et al. 2006). Taking all these previous steps into account, we investigated the effect of rotation on echelle diagrams.

The paper is organized as follows: in Section 2 for sake of notation, we briefly recall the frequency spacings and seismic diagnostics generally used for asteroseismic analysis of solar-like stars which will be considered in the following sections. Then, the equilibrium stellar models and their corresponding oscillation computations are described in Section 3. The validity of a perturbative modeling of the effects of rotation on oscillations in solar-like stars is discussed in Section 4. Section 5 describes the effects of rotation for seismic diagnostics based on echelle diagrams. A discussion of the results, including an illustration based on the solar-like star  $\eta$  Bootis and conclusions are given in Section 6.

## 2. Seismic diagnostics for internal structure

In the case of solar-like oscillations, modes with high radial order  $n$  are detected. In this regime, regular patterns are observed in the power spec-

trum which are related to internal properties of the star. Analysis of such characteristics allows us to infer information about various physical processes, particularly those that modify the sound speed and/or the Brunt-Väisälä frequency. Several frequency combinations are then used to analyze high-order p modes: large and small frequency spacings and their corresponding scaled counterparts, second-order frequency differences, and even high-order frequency differences (for a review on this topic see Goupil & Dupret 2007, and references therein).

### 2.1. Frequency spacings

The large (frequency) separation is hereafter denoted by  $\Delta\nu_{n,\ell}$  and defined by

$$\Delta\nu_{n,\ell} = \nu_{n,\ell} - \nu_{n-1,\ell}. \quad (1)$$

The large spacing is sensitive to surface layers where  $c_s$  is small, and hence oscillation modes spend more time there compared to the inner regions of the star. This spacing is generally studied in order to detect sharp variations of the sound speed, such as those at the base of the solar convection zone, or those resulting from the presence of ionization regions. The mean large spacing over several modes in the asymptotic regime scales with the dynamical time scale  $(R^3/GM)^{1/2}$  and is one of the pieces of information sought when constructing echelle diagrams.

The small (frequency) spacing, hereafter denoted by  $\delta\nu_{n,\ell}$ , is defined as follows

$$\delta\nu_{n,\ell} = \nu_{n-1,\ell+2} - \nu_{n,\ell}. \quad (2)$$

This spacing is sensitive to evolutionary effects (the age of the star for a given metallicity). Average large  $\langle\Delta\nu_{n,\ell}\rangle$  and small  $\langle\delta\nu_{n,\ell}\rangle$  spacings (over radial order  $n$ ) are used to estimate masses and ages of solar-like stars as first suggested by Christensen-Dalsgaard (1998).

In addition to the aforementioned frequency spacings, other frequency combinations are also used as efficient asteroseismic diagnostics:

$$\delta_{0,1}(n) = \nu_{n,0} - \frac{1}{2}(\nu_{n-1,1} + \nu_{n,1}) \quad (3)$$

$$\delta_{1,0}(n) = \frac{1}{2}(\nu_{n,0} + \nu_{n+1,0}) - \nu_{n,1}, \quad (4)$$

together with their corresponding scaled expressions

$$r_{0,1}(n) = \frac{\delta_{0,1}(n)}{\Delta\nu_{n+1,0}}, \quad r_{1,0}(n) = \frac{\delta_{1,0}(n)}{\Delta\nu_{n,1}}, \quad (5)$$

which are sensitive to inner stellar zones (Roxburgh & Vorontsov 2001; Mazumdar & Antia 2001; Roxburgh & Vorontsov 2003, see).

### 2.2. The Echelle Diagrams for asteroseismic diagnostics

One of the most frequently used techniques for seismic diagnostics of solar-like stars is the representation of the oscillation frequencies in the so-called echelle diagram (hereafter, ED). With such diagrams, one is able to identify the degree of modes and extract some information from the asymptotic properties mentioned above.

Echelle diagrams are constructed by cutting the oscillation spectrum into frequency slices of size  $\langle\Delta\nu_{n,\ell}\rangle$ , and stacking them up. Then the ED consists in depicting the oscillation frequencies as a function of the same frequencies modulo  $\langle\Delta\nu_{n,\ell}\rangle$ . In a first-order asymptotic regime, EDs should be composed of one vertical ridge per  $\ell$ , if modes are  $m$ -degenerate. When rotation is considered, each vertical ridge corresponds to a given  $(\ell, m)$  mode.

### 3. The seismic modeling

The present work has been undertaken with the use of two types of models: 1D-2D polytropes and 1D stellar models, the purpose and description of which are described in the following.

#### 3.1. Polytropes

Polytropic models are used in this work for the comparison between perturbative and non-perturbative approaches for the oscillation computations (section 4). This is so because, to date, no realistic (properly deformed by rotation) models of solar-like stars are yet available.

A polytropic model of index  $n = 3$  with  $M = 1.3 M_\odot$  and  $R = 1.276 R_\odot$  was considered as the reference model. From that model, 1D and 2D polytropic models with rotational velocities ranging from  $8 \text{ km s}^{-1}$  to  $48 \text{ km s}^{-1}$  were built (see Reese et al. 2006, for more details on 2D polytropes). The characteristics of all these models are listed in Table 1.

TABLE 1

CHARACTERISTICS OF THE  $1.30 M_{\odot}$  MODELS CONSIDERED IN THIS WORK (WITH THE EXCEPTION OF  $\mathcal{M}_{\eta}$  WHOSE MASS IS  $1.70 M_{\odot}$ ).  $\mathcal{P}_i$ , AND  $\mathcal{P}_i^{\dagger}$  ARE 1D AND 2D POLYTROPIC MODELS, RESPECTIVELY. STELLAR MODELS ARE DENOTED BY  $\mathcal{U}_i$  AND  $\mathcal{S}_i$ , FOR UNIFORM (CONSTANT ROTATION PROFILE AT GIVEN EVOLUTIONARY STAGE) AND SHELLULAR ROTATION (ROTATION PROFILE GIVEN BY EQ. 7) MODELS, RESPECTIVELY (DETAILS IN SECTION 3.3). MODEL SUBSCRIPTS  $i$  MAKE REFERENCE TO THE ROUND VALUE OF THE SURFACE ROTATIONAL VELOCITY IN  $\text{KMS}^{-1}$  (FOR  $\mathcal{M}_{\eta}$  THE ROTATIONAL VELOCITY IS  $30 \text{KMS}^{-1}$  APPROXIMATELY). THE RADIUS OF ALL THE MODELS IS  $R = 1.276 \pm 0.005 R_{\odot}$ . COLUMNS REPRESENT RESPECTIVELY, FROM LEFT TO RIGHT, THE AVERAGE LARGE SPACING, THE ACOUSTIC FREQUENCY  $\nu_{\text{ac}}$  (EQ. 11), THE VALUE OF  $\nu_{\text{max}}$  (EQ. 10), THE ROTATION FREQUENCIES IN BOTH THE SURFACE AND THE CENTER OF THE MODEL, AND THE SMALL NUMBERS  $\epsilon$  AND  $\mu$  (EQ. 9) THE LATTER BEING CALCULATED AT THE  $\nu_{\text{max}}$  FREQUENCY OF EACH MODEL.

Model	$\langle \Delta \nu_{n,\ell} \rangle$ $\mu\text{Hz}$	$\nu_{\text{ac}}$ $\text{mHz}$	$\nu_{\text{max}}$ $\text{mHz}$	$\Omega_{\text{s}}$ $\mu\text{Hz}$	$\Omega_{\text{c}}$ $\mu\text{Hz}$	$\epsilon$ $\times 10^{-2}$	$\mu(\nu_{\text{max}})$ $\times 10^{-3}$
$\mathcal{P}_0^{\dagger}$	98.40	-	-	0	0	0	-
$\mathcal{P}_8^{\dagger}$	98.40	-	-	1.43	1.43	1.85	-
$\mathcal{P}_{16}^{\dagger}$	98.40	-	-	2.92	2.92	3.70	-
$\mathcal{P}_{32}^{\dagger}$	98.40	-	-	5.84	5.84	7.40	-
$\mathcal{P}_{40}^{\dagger}$	98.40	-	-	5.84	5.84	9.26	-
$\mathcal{P}_{48}^{\dagger}$	98.40	-	-	8.75	8.75	11.11	-
$\mathcal{P}_8$	98.40	-	-	1.43	1.43	1.81	-
$\mathcal{P}_{16}$	98.40	-	-	2.92	2.92	3.70	-
$\mathcal{P}_{32}$	98.40	-	-	5.84	5.84	7.40	-
$\mathcal{P}_{40}$	98.40	-	-	7.24	7.24	9.16	-
$\mathcal{P}_{48}$	98.40	-	-	8.75	8.75	11.08	-
$\mathcal{U}_{08}$	108.60	3.79	2.25	1.47	1.47	1.86	0.66
$\mathcal{U}_{16}$	108.62	3.79	2.23	2.99	2.99	3.79	1.34
$\mathcal{U}_{32}$	108.65	3.79	2.24	5.75	5.75	7.28	2.58
$\mathcal{U}_{40}$	108.67	3.79	2.24	7.20	7.20	9.12	3.23
$\mathcal{U}_{48}$	108.70	3.80	2.24	8.58	8.58	10.84	3.83
$\mathcal{S}_8$	108.61	3.79	2.24	1.47	1.89	1.86	0.66
$\mathcal{S}_{16}$	108.64	3.79	2.23	2.92	3.79	3.69	1.30
$\mathcal{S}_{32}$	108.66	3.79	2.24	5.49	7.32	6.91	2.45
$\mathcal{S}_{40}$	108.69	3.79	2.24	7.29	9.69	9.24	3.27
$\mathcal{S}_{48}$	108.72	3.80	2.24	8.73	11.48	11.03	3.90
$\mathcal{M}_0$	109.12	3.79	2.25	0.00	0.00	0	0
$\mathcal{M}_{\eta}$	39.78	1.07	0.63	2.54	2.54	9.11	4.02

### 3.2. Stellar models

Equilibrium models were computed with the CESAM code (Morel 1997; Morel & Lebreton 2008). Our stellar models include the spherically averaged contribution of the centrifugal acceleration through an effective gravitational acceleration in the hydrostatic equation according to Kippenhahn & Weigert (1990). Specifically, the effective gravity is obtained as  $g_{\text{eff}} = g - \mathcal{A}_c(r)$ , where  $g$  is the local gravity,  $r$  the radius, and  $\mathcal{A}_c(r) = \frac{2}{3} r \Omega^2(r)$  the centrifugal acceleration (similar models have been previously used, for instance, by Goupil et al. 2000; Daszyńska-Daszkiewicz et al. 2002; Christensen-Dalsgaard & Thompson 1999; Suárez et al. 2006). Although the non-spherical components of the centrifugal acceleration are not considered in the equilibrium models, they are included in the oscillation computations by means of a linear perturbation analysis described in Dziembowski & Goode (1992), Soufi et al. (1998), and Suárez et al. (2006).

We consider two hypothesis about the internal rotation profile: uniform rotation (solid body rotation), and shellular rotation (radial differential rotation) with local conservation of the angular momentum during the evolution of the stellar model (see Suárez et al. 2006, for more details). The characteristics of both uniformly- and differentially-rotating models ( $\mathcal{U}_i$  and  $\mathcal{S}_i$ , respectively) are listed in Table 1. We consider rotational velocities for the models spanning the range of  $v \sin i$  observed in solar-like stars.

### 3.3. Oscillations computation

Oscillations were computed using the non-perturbative and perturbative approaches. The former consists in a numerical approach based on expansions of the equilibrium and oscillation variables on spherical harmonics for the angular dependence, and on Chebyshev polynomials for the radial dependence. Such computations were done for the 2D polytropic models described in Section 3.1.

For the perturbative approach, the adiabatic oscillation code FILOU was used (Suárez 2002; Suárez & Goupil 2008). This code corrects the oscillations frequencies up to the second-order effects of rotation. These include near degeneracy effects, which occur when two or more frequen-

cies are close to each other. More specifically, in order to remain in the hypothesis of the perturbative approach, we assume the loose condition that near degeneracy effects must be corrected for modes with frequencies satisfying:

$$|\nu_{nlm} - \nu_{n'l'm}| \lesssim \frac{1}{2} |\langle \Delta \nu_{n,\ell} \rangle|. \quad (6)$$

In addition, the frequency computation takes into account the presence of a radial differential rotation profile of the form

$$\Omega(r) = \bar{\Omega} \left( 1 + \eta_0(r) \right) \quad (7)$$

where  $\bar{\Omega}$  represents the angular rotational velocity at the surface and  $\eta_0(r)$  a radial function representing *shellular* rotation. This profile is only considered in the radiative zone, in which the rotation rate decreases approximately with a power of  $r$ , whereas instantaneous transport of the angular momentum is assumed in the convective core, implying thus a uniform rotation profile in that part of the star (an illustration of such a profile can be found in Suárez et al. 2009).

### 4. Validity of the perturbative approach for oscillation computations

The perturbative approach is considered valid when the parameters

$$\epsilon = \Omega / (GM/R^3)^{1/2} \quad (8)$$

$$\mu = \Omega / \nu_{n,\ell} \quad (9)$$

are small, that is, when (1) the stellar structure is not significantly deformed by the centrifugal force, and (2) oscillation frequencies are much larger than the angular rotation rate, respectively. More specifically, the stellar deformation, which scales as  $\epsilon^{1/2}$ , needs to be small in comparison to the mode wavelength, which scales as  $1/\nu_{n,\ell}$ . This implies that the use of a perturbative approach may fail when increasing the rotational velocity of the star, and this failure is expected to come first for high radial-order frequency modes, i.e. high frequency modes (Lignières et al. 2006; Reese et al. 2006).

It is thus relevant to investigate the validity of the perturbative approach for the oscillation computations, as well as to identify the possible effects that it may provoke on the echelle diagrams. To

do so, it is necessary to compare EDs constructed from synthetic oscillations computed with both approaches. In order to try to remain within the nominal limits of validity of perturbation theory, models were built with small values of  $\epsilon$  and  $\mu$ , around  $10^{-2}$  and smaller (see Table 1).

For the sake of shortness and simplicity, P and NP will indicate the perturbative and non-perturbative cases, respectively. For instance, echelle diagrams computed using the perturbative approach will be denoted by PEDs (Perturbative Echelle Diagrams), and those computed with a non-perturbative approach will be denoted by NPEDs (Non-Perturbative Echelle Diagrams). For both P and NP models, uniform rotation is assumed.

The comparison between both types of diagrams including all the  $m$  components of modes shows that these are very similar for rotational velocities lower than  $32 \text{ kms}^{-1}$  approximately (see Figure 1). For higher rotational velocities ( $\epsilon \gtrsim 0.09$ ), the P results should be interpreted with caution.

Nevertheless only slight differences (for this scaling, i.e. a few  $\mu\text{Hz}$ ) between PED and NPEDs come out for  $\ell = 0$  and  $\ell = 1, m = 0$  modes in the high-frequency region ( $\nu_{n,\ell} > 2 \text{ mHz}$ ). This means that, at the scale of echelle diagrams, both P and NP can be considered as quasi-identical. This is also the case when comparing the P and NP large frequency spacing.

For the small spacings, we find very similar results from both approaches, as can be deduced from the comparison between the top and bottom panels in Figure 2. For  $\delta\nu_{0,2}$ , P spacings show the same behavior as a function of the frequency as their NP counterparts. Indeed, the results are quasi-identical for models with rotational velocities up to  $40 \text{ kms}^{-1}$ . Deviations of P with respect to NP spacings are more evident for  $48 \text{ kms}^{-1}$ , showing differences of around  $1 \mu\text{Hz}$ , which are visible for frequencies higher than  $1.5 \text{ mHz}$  and which increase with the oscillation frequency. Similarly, the analysis of P and NP results for  $\delta\nu_{1,0}$  are similar, with increasing differences from  $1.5 \text{ mHz}$  to higher frequencies.

Furthermore, when near degeneracy effects are not considered, the resulting small spacings deviate from the NP results even for the lowest ro-

tational velocities considered here. This is shown in Figure 2 (middle panels), where it can be seen that such deviations increase with the frequency and the rotational velocity. This can be explained by the dependency of the near-degeneracy correcting terms upon, among other terms, the frequency, the rotation profile, and structure terms affected by the centrifugal force (Suárez et al. 2006). This issue, together with a more detailed and quantitative comparison, is currently in progress, and the results will be published in a forthcoming paper (Ouazzani et al. 2010, in prep.).

Several important consequences can be extracted from these results: (1) It is correct to use the P approach for studying the effect of rotation on EDs (up to  $\epsilon = 0.09$ ), (2) even for low rotational velocities, second-order effects of rotation, including near degeneracy effects, must be included in the oscillation computations, and (3) there are no artificial features in the PEDs which could jeopardize the correct physical interpretation of the seismic diagnostics performed with them (even at a small scale) as long as near degeneracy effects are properly taken into account.

## 5. EDs of stellar models

Following the conclusions on the validity of the perturbation methods given in the previous section, we computed the oscillations of the  $\mathcal{U}_i$  and  $\mathcal{S}_i$  models (Table 1) including near degeneracy effects. It can be shown that EDs of  $\mathcal{S}_i$  and  $\mathcal{U}_i$  models are very similar, so for simplicity, discussion will be focused on  $\mathcal{U}_i$  models. For brevity, ridges in the EDs are specified with the notation  $(\ell, m)$ .

Figure 3 shows the echelle diagrams calculated for the three  $\mathcal{U}_i$  models of Table 1. At first sight, one notices that second-order effects of rotation do not change substantially the overall shape of the EDs, which remains dominated by the internal stratification of the star and the presence of hydrogen and helium ionization zones. However, significant variations (within the global ED structure) are found for increasing rotation rates  $\Omega$ , and for different frequency domains. In fact, such variations should be considered in terms of  $(\epsilon, \mu)$  values, rather than a function of the rotational velocity. It can be shown, for instance, that for similar rotational velocities but different masses, EDs show different results. Here, for clarity, the discussion

is nevertheless held with respect to  $v_{\text{rot}}$ .

For  $\mathcal{U}_{08}$ , the multiplets with different  $\ell$  remain quite distant from each other. In particular the frequency gap between the  $\ell = 0$  and 2 multiplets is around  $20 \mu\text{Hz}$ , and between the  $\ell = 1, 3$  multiplets around  $10 \mu\text{Hz}$ . This roughly corresponds to the spacing between  $m = 0$  ridges for those multiplets. For such a low rotational velocity, first-order effects of rotation, which are proportional to  $m\Omega$ , dominate, thereby explaining the symmetry of the multiplets. In this case, the rotational splitting is  $1.47 \mu\text{Hz}$  (see Table 1), which represents approximately the 7% and 14% of the average distance between the 0-2 and 1-3 multiplets, respectively, and even more importantly, about 1% of the ED scale ( $120 \mu\text{Hz}$ ).

For  $\mathcal{U}_{16}$ , however, the symmetry of multiplets is broken for frequencies greater than  $1.5\text{mHz}$  approximately, indicating that, from rotational velocities around  $16 \text{kms}^{-1}$ , second-order effects of rotation become important. Nevertheless, such effects are not strong enough to mix up multiplets of different mode degrees, whose centroid modes are separated (in average) by about  $10 \mu\text{Hz}$  (0-2 multiplets) and  $20 \mu\text{Hz}$  (1-3) multiplets. However, the rotational splitting for this model is  $3 \mu\text{Hz}$  and the  $m$  ridges are almost two times (in average) more spread in the ED than those of model  $\mathcal{U}_{08}$ . Consequently, the identification of the mode degree is not so obvious in this case: The (1,+1) ridges are closer to (3,-3) as the frequency increases (around  $4 \mu\text{Hz}$  at  $\nu_{n,\ell} \simeq 1.5\text{mHz}$ , and  $2 \mu\text{Hz}$  at  $\nu_{n,\ell} \simeq 3\text{mHz}$ ). Similarly, radial modes ridges are close to (2,-2) ones (less than  $5 \mu\text{Hz}$ ). This is particularly relevant for the highest frequency domain.

But the most extreme case considered here is the  $\mathcal{U}_{32}$  model. With such a large rotation rate, second-order effects including near degeneracy effects (see Section 3.2) become significant. From Figure 3, one notices that there is a blend of ridges which might blur the typical ED features, in particular when few modes are detected. The scenario described for  $\mathcal{U}_{16}$  is somehow intensified now. The blending is caused by ridges approaching, and even crossing each other in certain cases: The (1,-1) ridge crosses (1,0) at  $\nu_{n,\ell} \simeq 1.5\text{mHz}$ . Similarly, (2,-2) crosses the radial modes at  $\nu_{n,\ell} \simeq 1.8\text{mHz}$ . Moreover, (3,- $m$ ) are very close to any of the (1, $m$ ) ridges, e.g. (3,-1) with (1,+1), (3,-2) with

(1,+1), and (3,-3) with both (1,+1) and (3,+2). In such a case, unless one has good independent reasons to assume that only  $m=0$  modes are detected, it would be extremely difficult to attribute a ( $\ell, m$ ) value to some of the modes.

## 6. Discussion & conclusions

We showed that that even for mild rotation, second-order effects of rotation start to have significant impact on the oscillation frequencies in the range of their expected maximal detection, that is around  $\nu_{\text{max}}$ , i.e. the frequency at which the observed power spectrum reaches its maximum. Here, we use the empirical relation calibrated to solar values (Bedding et al. 2004) can be written as

$$\nu_{\text{max}} = \nu_{\text{max},\odot} \frac{\nu_{\text{ac}}}{\nu_{\text{ac},\odot}}, \quad (10)$$

where  $\nu_{\text{ac}}$  is the acoustic cut-off frequency defined by

$$\nu_{\text{ac}} = c/H_{\text{p}} \quad (11)$$

where  $H_{\text{p}}$  is the pressure scaleheight. We assumed the value for the solar calibration  $\nu_{\text{ac},\odot}/\nu_{\text{max},\odot} \sim 1.70$  (Balmforth & Gough 1990). Indeed, rotation effects on EDs (see Figure 3) are of the order of the  $\mu\text{Hz}$  for rotational velocities higher than  $8 \text{kms}^{-1}$  ( $\epsilon \sim 0.018$ ,  $\mu(\nu_{\text{max}}) \sim 0.6$ ) for frequencies around  $\nu_{\text{max}}$  (see Table 1) and higher.

### 6.1. Mode identification

From the above results, one question naturally arises: How can we distinguish between different  $m$  ridges when they are close or even crossing each other? This question has no easy answer. There are many physical variables that must be considered when analyzing mode excitation and detection: geometry, visibility, intrinsic amplitudes, excitation mechanisms, etc. It is not the purpose of this work to go into great detail on these aspects, however, analysis of Fig 3 can provide some hints which could help with mode identification. For instance, notice that  $-m$  ridges spread more drastically than the  $+m$  ones, this effect being more significant as the rotation velocity increases. This would thus help to identify the  $m \neq 0$  components of the oscillation spectra, in particular in the case for which this differential behaviour is stronger, i.e. for the  $\ell = |m|$  modes. In fact, based on visibility and geometrical considerations, those modes

are more visible for increasing inclination angles, the limit case being  $i \rightarrow 90$  deg, that is when the star is being observed equator-on. Furthermore, it has been found empirically that observed amplitudes for p modes in main sequence stars are correlated with increasing  $i$  (Suárez et al. 2002). This result was then supported by theoretical simulations using non-perturbative theory for the oscillation computations (Lignières et al. 2006) which predict that the mode amplitude tends to concentrate near the equator (firstly predicted by Clement 1998). It can thus be concluded that the larger the rotational velocity of the star is, the more chances the observed ridges in EDs correspond to  $\ell = 0$  and/or  $\ell = |m|$  modes.

## 6.2. High frequency range and surface effects

Second-order effects of rotation increase with the frequency and are therefore largest in the high frequency domain (above  $\nu_{max}$ ) where frequencies are sensitive to various surface effects (see Goupil & Dupret 2007, for a review on these effects). For instance, Straka et al. (2006) showed that turbulence causes variations in the upper part (highest-frequencies) of EDs. In that work, a comparison of classical models without turbulence with models including 3D simulations of turbulence reveals that differences in frequency for radial modes of about  $5 \mu\text{Hz}$  (from  $\nu_{max}$  to higher frequencies) between the two types of models can exist (see EDs of Figs. 4 and 5 in Straka et al.). These orders of magnitude are comparable to those we find here for models with rotational velocities of about  $16 \text{ km s}^{-1}$  in the equivalent frequency domain.

Similarly, it has been shown (Théado et al. 2005; Castro & Vauclair 2006) that the effects on the model frequencies with and without including such diffusion processes are different for radial modes than for non-radial modes thereby affecting the small spacings. Such effects can reach a few  $\mu\text{Hz}$  for a model of  $1.30 M_{\odot}$ . This means that, rotational second-order effects shown in the EDs of Figure 3 can be larger than those coming from microscopic diffusion of He even for very small rotational velocities. Rotation can thus be considered as another contribution to such surface effects, like turbulence. Note however that rotation effects extend to smaller frequencies for

higher rotation rates.

Scaled small frequency spacings like  $r_{1,0}$  (see Section 2.1) have been shown to be rather insensitive to surface effects, and therefore can probe properties of the inner part, like the convective core overshoot (Roxburgh & Vorontsov 2003, 2004). This is no longer true when rotation is responsible for the 'surface effects'. Indeed we find a similar behavior of both spacings  $r_{1,0}$  and  $\delta\nu_{1,0}$  (Figs. 4c and 4b, respectively). The reason is that the effects of rotation on EDs are mainly explained by the variations in the small spacings. These variations become significant when the rotational velocity and oscillation frequency increase (see Figs. 2.1a & 2.1b,) but they are not compensated by the effects on large spacings which remain quite small. This is confirmed with a calculation of the  $r_{1,0}$  removing the effect of the stellar distortion by the centrifugal force from the oscillations frequencies, i.e. we neglect the second-order terms in the perturbation treatment. Then, all the curves in Figure 4c collapse (Figure 4d).

These results imply that even at small stellar rotational velocities (from  $10\text{-}15 \text{ km s}^{-1}$ ), the scaled  $r_{\ell,n}$  spacings are sensitive to the stellar distortion, therefore care must be taken when using them as indicators for probing the stellar interior. It is possible to find appropriate combinations of frequencies which enable to remove 'pollution' due to second-order effects of rotation in  $r_{1,0}$  and  $\delta\nu_{1,0}$  (Dziembowski & Goupil 1998; Goupil et al. 2004; Lochard 2005)

## 6.3. An illustration: the solar-like star $\eta$ Bootis

In order to illustrate how rotation affects the asteroseismic diagnostics of real data, we selected the well-known solar-like star  $\eta$  Bootis (HD HR5235) which has a measured  $v \sin i$  of  $12.8 \text{ km s}^{-1}$  (Bouchy & Carrier 2002). This bright sub-giant G0 star has been the subject of many observational and interpretation works in the literature. One of the most recent works on theoretical interpretation of this star was published by Carrier et al. (2005) (hereafter C05). In that work, a detailed asteroseismic modeling of the star, including rotation and atomic diffusion, was performed. For illustrative purposes, we computed stellar models which are approximately similar to some of the representative models listed in



Table 5 of the aforementioned paper. The physical parameters and the observed oscillation frequencies of the star were taken from C05.

As shown in the previous sections, shellular rotation and uniform rotation profiles yield almost identical results at the scale of EDs. Thus, in order to simplify the procedure, we adopt, for the present illustration, the hypothesis of uniform rotation. For the convection description, the mixing-length formulation is used, assuming an overshoot of 0.2. The physical parameters and the observed oscillation frequencies of the star were also taken from C05.

We searched for models matching the observed frequencies and the large spacing estimated by C05 ( $\langle \Delta\nu_{n,\ell} \rangle = 39.9 \mu\text{Hz}$ ) with the help of EDs. To do so, stellar models with rotational velocities ranging from  $12 \text{ km s}^{-1}$  ( $i \rightarrow 90 \text{ deg}$ ) and  $48 \text{ km s}^{-1}$  ( $i \rightarrow 14 \text{ deg}$ ) were computed. This range of rotational velocities ensures the use of a perturbative approach for the oscillation computations (see discussion of the perturbative approach in Section 4).

Assuming that most detected modes are  $m = 0$  modes, the best diagnostics for the large separation ( $\langle \Delta\nu_{n,\ell} \rangle = 39.78 \mu\text{Hz}$ ) were obtained for a model,  $\mathcal{M}_\eta$ , with similar characteristics to model M3 of C05, i.e., a mass of  $1.70 M_\odot$  with radius  $R = 2.79 R_\odot$ , and an age of  $2.25 \text{ Gyr}$  ( $T_{\text{eff}} = 6014 \text{ K}$ ,  $L = 9.14 L_\odot$ ), and surface rotational velocity of  $30 \text{ km s}^{-1}$  (which implies an inclination angle of  $i \sim 25^\circ$ ). A value  $\alpha = 1.75$  is taken for the MLT mixing length parameter. The chemical composition is fixed at  $X = 0.7, Z = 0.03$ . Additional characteristics of this model are listed in Table 1.

The resulting ED for  $\mathcal{M}_\eta$  fits reasonably well the  $m = 0$  modes with the observations (see Figure 5a) whereas for a lower rotation velocity set at  $21 \text{ km s}^{-1}$ , the match is poorer and the stellar model would not be considered as a good match in absence of rotation (Figure 5b), particularly for the  $\ell = 1, m = 0$  modes. Even when rotation is included, the mode identification is not unique. Note that the (1,-1), (3,-3), and (3,-2) ridges are very close to (1, 0), which is also the case of (1, +1) with (3, 0). Similarly, we found that the ridges (2, -2) and (2, -1) are almost coincident with (0, 0), and the (2, +2) with (2, 0). Some of the high-frequency modes ( $\nu_{n,\ell} \geq 0.85 \text{ mHz}$ ) are better fit with  $m \neq 0$  ridges. For the selected model, these modes are hardly fit when rotation

effects are not included in the modeling, as shown in panel b of Figure 5. In any case, we are aware that the presence of all  $m$  components makes the ED more dense. This increases the probability of a better match and non-uniqueness of the solution, in particular when no independent mode identification information is available. Model fine tuning should thus consider variations of both the amount and the shape of the rotation profile.

Quantitatively, the effects of rotation found reach  $5 \mu\text{Hz}$  approximately in certain cases (e.g. for  $\ell = 1$  modes) when considering only  $m = 0$  modes, but this is largely increased when fitting  $m \neq 0$  ridges. In general, these effects are much larger than the observational uncertainties. Since no information on individual frequency uncertainties are given in C05, the observational uncertainties shown in Figure 5 correspond to the uncertainty of the observational  $\delta\nu_{0,2}$  small spacings given in that work, i.e. around  $1 \mu\text{Hz}$  ( $\delta\nu_{0,2}$  corresponds to the mean separation between the  $\ell = 0$  and 2 ridges). Note that it is possible that the present solution including rotation may not be unique. For instance, small variations around the physical characteristics of  $\mathcal{M}_\eta$  (mass, effective temperature, gravity, angular momentum distribution, etc.) may yield similar fits. It can be shown that variations in the physical characteristics of  $\mathcal{M}_\eta$  must be small in order fit the observations as shown in Figure 5. This is coherent with an echelle diagram of an evolved star (in the main sequence) as it is predicted by model  $\mathcal{M}_\eta$ . This explains also that small variations of the modulo, around  $0.01 \mu\text{Hz}$  affect significantly to the accuracy of the fit.

Depending on the star characteristics, the impact on precise seismic diagnostics and thereby on accurate modeling varies. For very small rotational velocities, i.e.  $v \sin i \leq 5 \text{ km s}^{-1}$ , rotation effects can be neglected. However, for higher  $v \sin i$ , the modeling should be performed taking the second-order (distortion) effects into account. Special caution must be taken when no additional information about the angle of inclination of the star is available (and/or the rotational splitting), otherwise the accuracy of the modeling may be compromised significantly. This, combined with additional information coming from spectroscopy and/or multicolor photometry, may be helpful for the identification of modes in solar-

like stars (Suárez et al., work in progress using *CoRoT* data).

This example illustrates well that for solar like oscillating, low and intermediate mass main sequence stars with rotation rates in the upper part of the observed rotation rate range, the modeling should be performed taking full second-order (distortion) effects into account. Hence, special caution must be taken when no additional information about the angle of inclination of the star is available (and/or the rotational splitting), otherwise the accuracy of the modeling may be significantly compromised if the rotation of the star happens to be large despite a small  $v \sin i$ .

JCS acknowledges support from the "Instituto de Astrofísica de Andalucía (CSIC)" by an "Excellence Project post-doctoral fellowship" financed by the Spanish "Conjunción de Innovación, Ciencia y Empresa de la Junta de Andalucía" under project "FQM4156-2008". JCS also acknowledges support by the Spanish "Plan Nacional del Espacio" under project ESP2007-65480-C02-01, and financial support from CNES. DRR acknowledges support from the CNES through a post-doctoral fellowship.

## REFERENCES

- Appourchaux, T., Michel, E., Auvergne, M., et al. 2008, *A&A*, 488, 705
- Baglin, A. 2003, *Advances in Space Research*, 31, 345
- Balmforth, N. J. & Gough, D. O. 1990, *ApJ*, 362, 256
- Bedding, T. R., Kjeldsen, H., Butler, R. P., et al. 2004, *ApJ*, 614, 380
- Belkacem, K., Samadi, R., Goupil, M., et al. 2009, *Science*, 324, 1540
- Bouchy, F. & Carrier, F. 2002, *A&A*, 390, 205
- Carrier, F., Eggenberger, P., & Bouchy, F. 2005, *A&A*, 434, 1085
- Castro, M. & Vauclair, S. 2006, *A&A*, 456, 611
- Christensen-Dalsgaard, J. 1998, *Lecture notes on Stellar Oscillations*, fourth edition edn. (Institut for Fysikk og Astronomi, Aarhus University: Christensen-Dalsgaard J.)
- Christensen-Dalsgaard, J. & Thompson, M. J. 1999, *A&A*, 350, 852
- Clement, M. J. 1998, *ApJS*, 116, 57
- Cunha, M. S. & Metcalfe, T. S. 2007, *ApJ*, 666, 413
- Daszyńska-Daszkiewicz, J., Dziembowski, W. A., Pamyatnykh, A. A., & Goupil, M.-J. 2002, *A&A*, 392, 151
- De Ridder, J., Barban, C., Baudin, F., et al. 2009, *Nature*, 459, 398
- Dziembowski, W. A. & Goode, P. R. 1992, *ApJ*, 394, 670
- Dziembowski, W. A. & Goupil, M.-J. 1998, in *The First MONS Workshop: Science with a Small Space Telescope*, held in Aarhus, Denmark, June 29 - 30, 1998, Eds.: H. Kjeldsen, T.R. Bedding, Aarhus Universitet, 69
- Gilliland, R. L., et al. 2010, *PASP*, 122, 131
- Gough, D. 1987, *Nature*, 326, 257
- Goupil, M. J. 2009, in *Lecture Notes in Physics*, Berlin Springer Verlag, Vol. 765, *Lecture Notes in Physics*, Berlin Springer Verlag, ed. J.-P. Rozelot & C. Neiner, 45–99
- Goupil, M. J. & Dupret, M. A. 2007, in *EAS Publications Series*, Vol. 26, *EAS Publications Series*, ed. C. W. Straka, Y. Lebreton, & M. J. P. F. G. Monteiro, 93–110
- Goupil, M.-J., Dziembowski, W. A., Pamyatnykh, A. A., & Talon, S. 2000, in *Delta Scuti and Related Stars, Reference Handbook and Proceedings of the 6th Vienna Workshop in Astrophysics*, held in Vienna, Austria, 4-7 August, 1999. *ASP Conference Series*, Vol. 210. Edited by Michel Breger and Michael Montgomery. (San Francisco: ASP) ISBN: 1-58381-041-2, 2000., p.267, 267
- Goupil, M. J., Samadi, R., Lochard, J., Dziembowski, W. A., & Pamyatnykh, A. 2004, in *ESA SP-538: Stellar Structure and Habitable Planet Finding*, 133

- Goupil, M. J. & Talon, S. 2002, in ASP Conf. Ser. 259: IAU Colloq. 185: Radial and Nonradial Pulsations as Probes of Stellar Physics, 306–+
- Kippenhahn, R. & Weigert, A. 1990, "Stellar structure and evolution", Astronomy and Astrophysics library (Springer-Verlag)
- Lignières, F., Rieutord, M., & Reese, D. 2006, *A&A*, 455, 607
- Lochard, J. 2005, Ph.D. Thesis, Paris XI University, Observatoire de Paris.
- Mathis, S., Palacios, A., & Zahn, J.-P. 2007, *A&A*, 462, 1063
- Matthews, J. M. 1998, in Structure and Dynamics of the Interior of the Sun and Sun-like Stars SOHO 6/GONG 98 Workshop Abstract, June 1-4, 1998, Boston, Massachusetts, ESA Publications Division, European Space Agency, Noordwijk, The Netherlands, Vol. 6, 395
- Mazumdar, A. & Antia, H. M. 2001, *A&A*, 377, 192
- Michel, E., Baglin, A., Auvergne, M., et al. 2008, *Science*, 322, 558
- Morel, P. 1997, *A&AS*, 124, 597
- Morel, P. & Lebreton, Y. 2008, *Ap&SS*, 316, 61
- Ouazzani, R., Goupil, M. J., Suárez, J. C., & Dupret, M. A. 2009, *A&A*, in prep.
- Reese, D., Lignières, F., & Rieutord, M. 2006, *A&A*, 455, 621
- Roxburgh, I. W. & Vorontsov, S. V. 2001, *MNRAS*, 322, 85
- Roxburgh, I. W. & Vorontsov, S. V. 2003, *A&A*, 411, 215
- Roxburgh, I. W. & Vorontsov, S. V. 2004, in ESA Special Publication, Vol. 538, Stellar Structure and Habitable Planet Finding, ed. F. Favata, S. Aigrain, & A. Wilson, 403–406
- Soufi, F., Goupil, M. J., & Dziembowski, W. A. 1998, *A&A*, 334, 911
- Straka, C. W., Demarque, P., Guenther, D. B., Li, L., & Robinson, F. J. 2006, *ApJ*, 636, 1078
- Suárez, J. C. 2002, Ph.D. Thesis, ISBN 84-689-3851-3, Paris VII (Denis Diderot) University.
- Suárez, J.-C., Michel, E., Pérez Hernández, F., et al. 2002, *A&A*, 390, 523
- Suárez, J. C. & Goupil, M. J. 2008, *Ap&SS*, 316, 155
- Suárez, J. C., Goupil, M. J., & Morel, P. 2006, *A&A*, 449, 673
- Suárez, J. C., Moya, A., Amado, P. J., Martín-Ruiz, S., Rodríguez-López, C., & Garrido, R. 2009, *ApJ*, 690, 1401
- Teixeira, T. C., Kjeldsen, H., Bedding, T. R., et al. 2009, *A&A*, 494, 237
- Théado, S., Vauclair, S., Castro, M., Charpinet, S., & Dolez, N. 2005, *A&A*, 437, 553

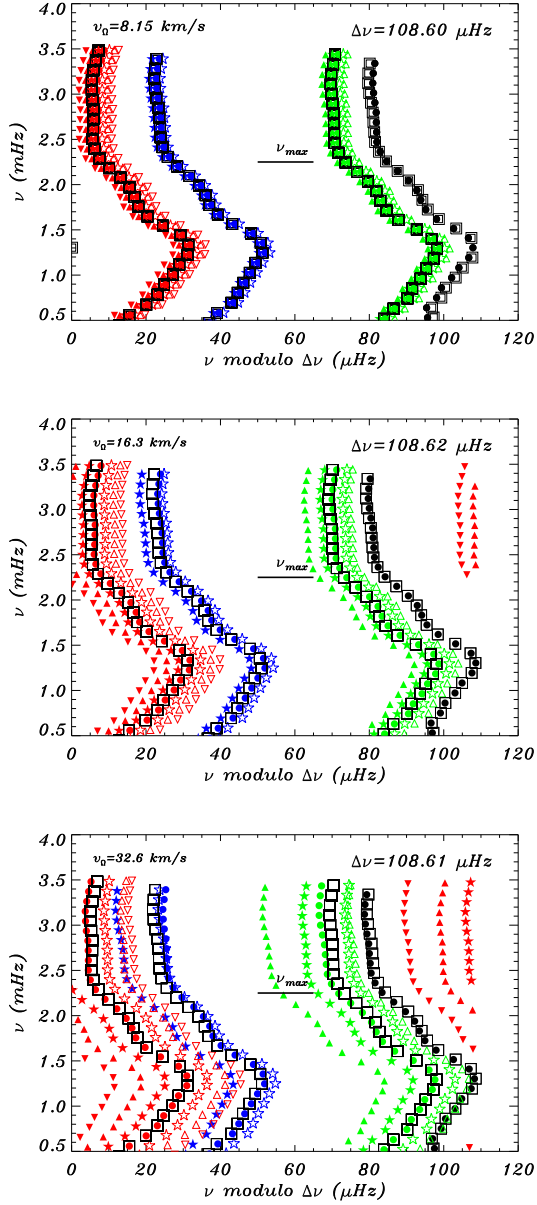


Fig. 3.— Echelle diagrams for the uniformly-rotating models  $\mathcal{U}_i$ . Open squares correspond to ridges of the non-rotating stellar model  $\mathcal{M}_0$ . The remaining symbols and colors have the same meaning as in Figure 1. The small horizontal line shows the location of the  $\nu_{\max}$  frequency. Stars, triangles, and inverted triangles represent modes with  $|m| = 1, 2,$  and  $3,$  respectively. (For clarity, colors are used in the *on-line* version of the paper).

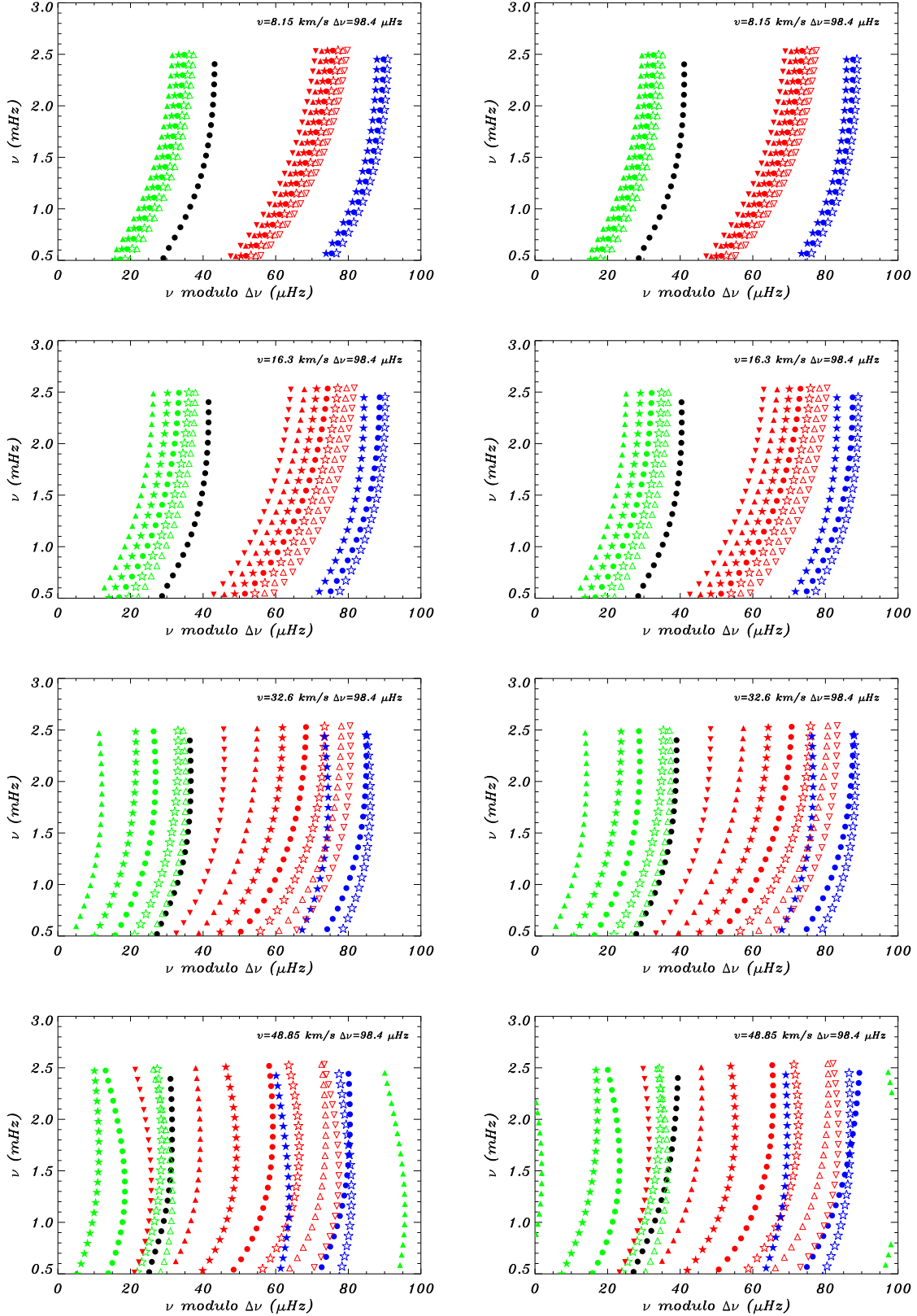


Fig. 1.— Perturbative (right panels) and non-perturbative (left panels) echelle diagrams computed for a polytropic model with four different rotational velocities (increase from top to bottom). Black and green symbols represent  $\ell = 0$  and  $\ell = 2$  modes, respectively. Blue and red symbols represent  $\ell = 1$  and  $\ell = 3$  modes, respectively. Filled circles represent both  $\ell = 0$  and  $m = 0$  modes. For the rest of modes, filled and

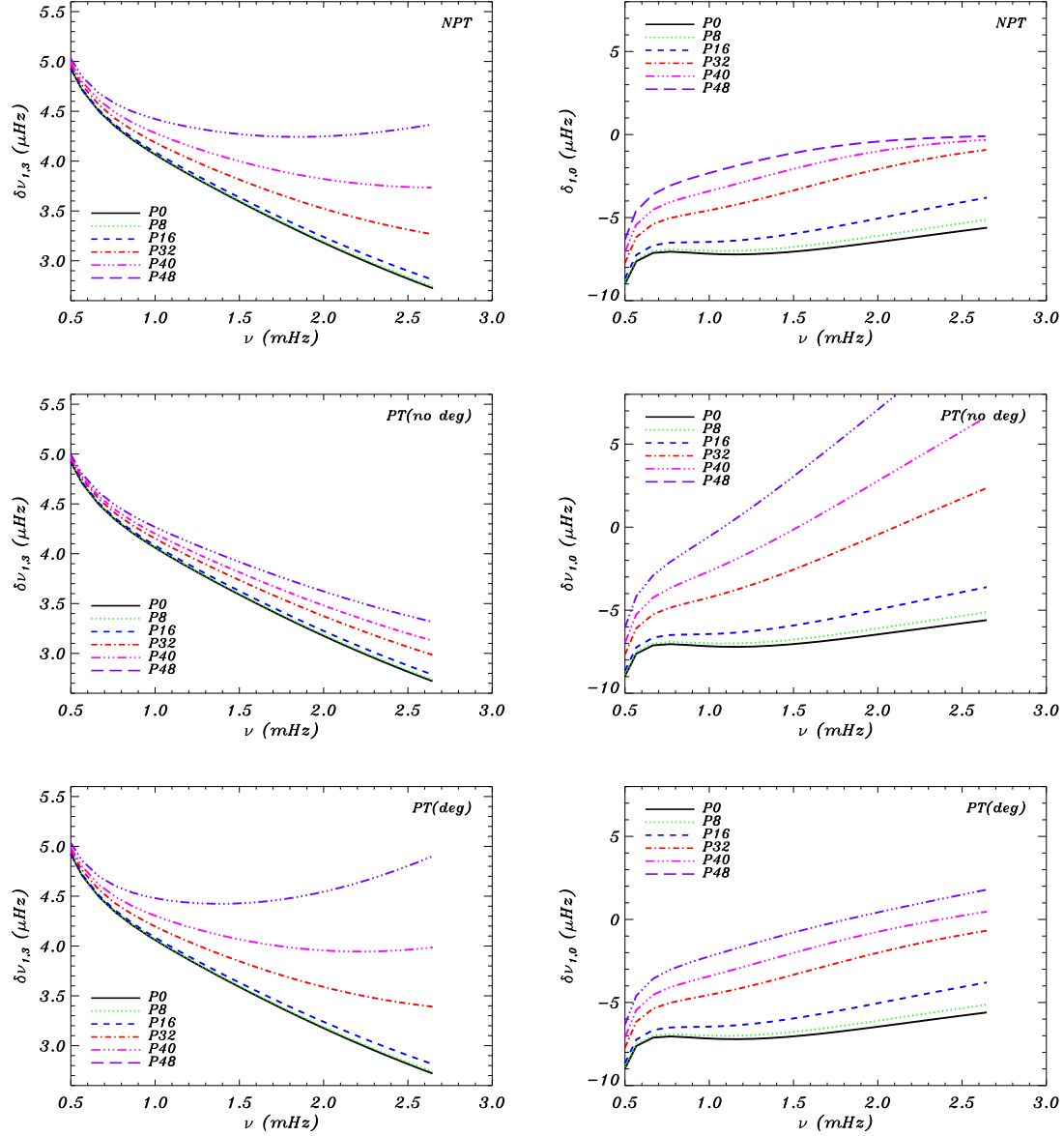


Fig. 2.— Small spacings  $\delta\nu_{0,2}$  (left panels) and  $\delta\nu_{0,1}$  (right panels) as a function of the oscillation frequency. Panels on top correspond to NP oscillations. Middle panels show spacings calculated with a perturbative approach without including near-degeneracy effects. Bottom panels are similar to middle panels but near-degeneracy is included. Different line types correspond to spacings computed for different rotational velocities. Colored figures are available in the on-line version of the paper.

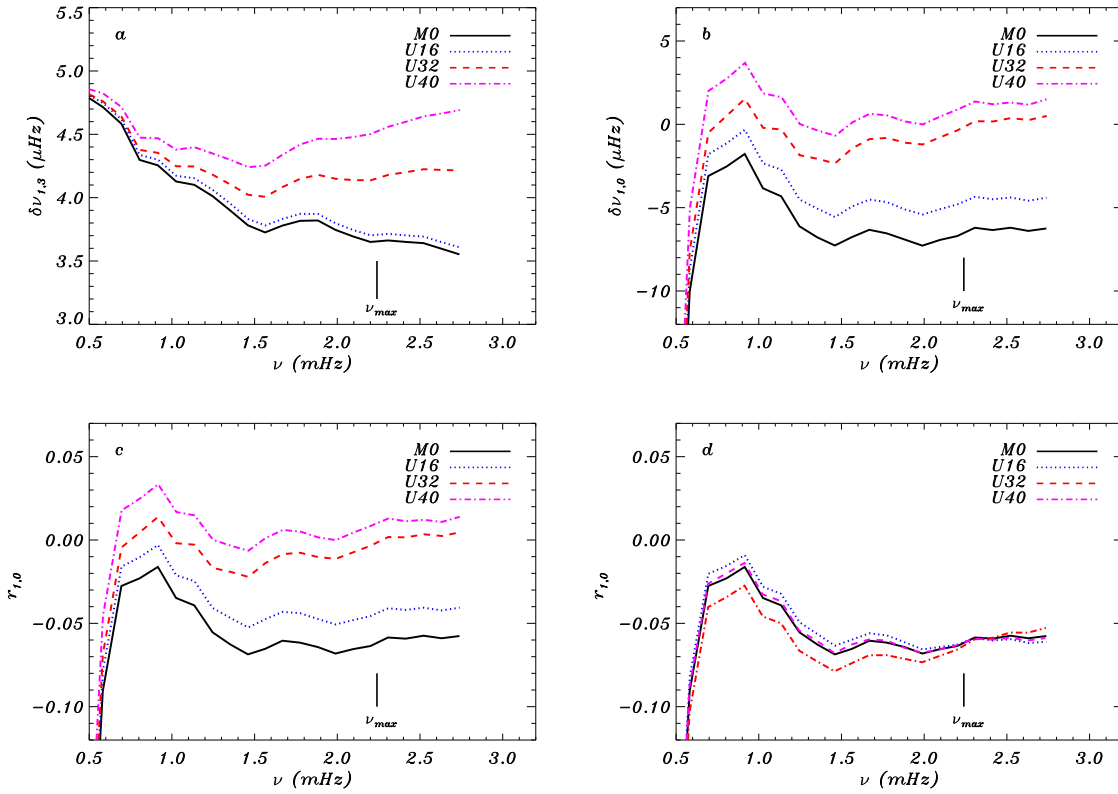


Fig. 4.— Effects of rotation on different small frequency spacings represented as function of the oscillation frequency. Panel (a), and (b) show the small frequency spacings  $\delta\nu_{1,3}$  and  $\delta\nu_{1,0}$ , respectively. Panel (c) and (d) show the scaled spacings  $r_{1,0}$ , the latter being calculated without taking second-order effects of rotation into account. The small vertical line indicates the location of the  $\nu_{\max}$  frequency.

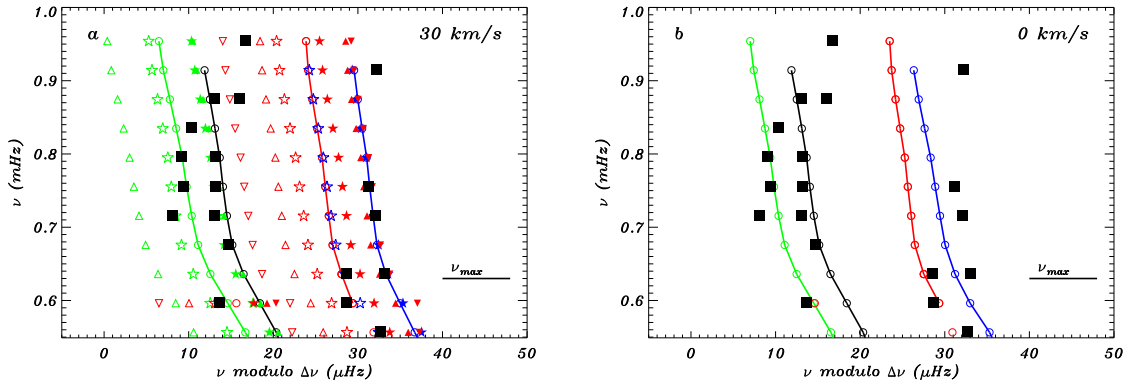


Fig. 5.— Illustration of considering rotation effects on echelle diagrams (a) for the seismic diagnostics for the solar-like star  $\eta$  Bootis (oscillation frequencies taken from C05) compared with the non-rotating case (b). The observed frequencies are represented by black filled squares. The nomenclature used to represent the theoretical frequencies in previous figures is also adopted here. For the sake of clarity, the  $m = 0$  as well as the radial modes are connected with lines. Note the presence of mixed modes at low frequency (near 0.6 mHz). For the simplicity of the whole figure, these modes are not connected by lines. The uncertainty of the observed frequencies,  $1 \mu\text{Hz}$  approximately, were roughly estimated from those of the small spacings given in C05 (more details in the text). This is approximately the size of the symbols. Stars, triangles, and inverted triangles represent modes with  $|m| = 1, 2,$  and  $3,$  respectively.